THE JOURNAL OF PHYSICAL CHEMISTRY B

Article

pubs.acs.org/JPCB

Determination of Size of Molecular Clusters of Ethanol by Means of NMR Diffusometry and Hydrodynamic Calculations

Mária Šoltésová,[†] Ladislav Benda,[†,‡] Mikuláš Peksa,[†] Jiří Czernek,[§] and Jan Lang*[,†]

[†]Department of Low Temperature Physics, Faculty of Mathematics and Physics, Charles University in Prague, V Holešovičkách 2, CZ-18000 Prague 8, Czech Republic

[‡]Institut für Chemie, Technische Universität Berlin, Straße des 17. Juni 135, DE-10623 Berlin, Germany

[§]Institute of Macromolecular Chemistry, Academy of Sciences of the Czech Republic, Heyrovského náměstí 2, CZ-16206 Prague 6, Czech Republic

Supporting Information

ABSTRACT: The microscopic structure of ethanol in the liquid state is characterized as a dynamic equilibrium of hydrogen-bonded clusters of different sizes and topologies. We have developed a novel method for determination of the average size of the clusters that combines the measurement of diffusion coefficient by means of NMR diffusometry technique and hydrodynamic simulations. The approach includes the use of HydroNMR [J. Garcìa de la Torre, M. L. Huertas, and B. Carrasco, J. Magn. Reson. *147*, **2000**, 138] for small molecules, which is attained here by the calibration procedure using a dilute solution of tetramethylsilane. It is thus possible to correlate the experimentally determined diffusion coefficient of ethanol with calculated diffusion coefficients of the modeled clusters of different sizes. We found that average size of the clusters in 0.16 M solution of ethanol in *n*-hexane corresponds to the monomer above 300 K and to the pentamer/hexamer below 240 K. The clusters in the case of 0.44 M solution are generally slightly larger, from the average size corresponding to the dimer at 320 K and the hexamer at 210 K.

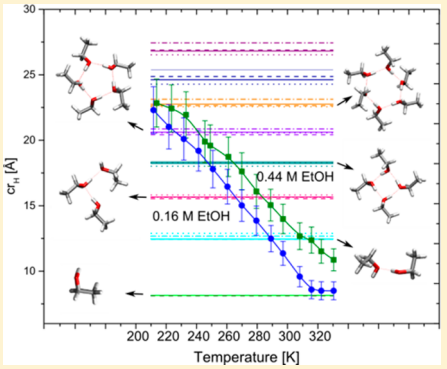

I. INTRODUCTION

Ethanol forms molecular clusters held together by hydrogen bonds between the hydroxyl groups (Figure 1). This phenomenon has been studied for more than 60 years using a vast variety of methods. This topic was recently comprehensively reviewed by Suhm, focusing mainly on spectroscopy of cold molecular aggregates produced by adiabatic gas expansion or supersonic jets.[1] The details of clusters' structure and dynamics in the liquid state remain open and various published results are often contradictory (vide infra).

Ethanol clusters may contain various numbers of monomeric units. We will denote this quantity as "the size of the cluster" further on for simplicity. Hydrogen donor−acceptor properties of alcohol hydroxyl groups are determinant for the topology of the clusters. The size and topology of the alcohol clusters present in the liquid state are the examples of the open questions.

The effect of hydrogen bonding on the chemical shift of the hydroxyl group in ^{1}H NMR spectrum was recognized as early as in 1951.[2,3] There have been many attempts to interpret the concentration and temperature dependencies of ^{1}H chemical shift in terms of the size of clusters. For example, Saunders and Hyne[4] reported that their data for ethanol dissolved in CCl_4 corresponded best to the monomer−tetramer equilibrium.

The hydroxyl groups of ethanol molecules may adopt gauche (G) or trans (T) rotameric states. Dyczmons[5] presented a detailed theoretical study of the possible monomer and dimer geometries. While the trans conformation is the minimum for the monomer, two gauche units appear to be the global minimum for the dimer. Nevertheless, the author identified a total number of 24 stable conformations for the dimer in vacuum. Dyczmons' work documents the major challenge of the microscopic structural characterization of the ethanol clusters: the number of conceivable states grows fast with the number of molecular units involved in the cluster, thus many geometries may be populated for the cluster of given size. Further, the clusters larger than dimers may adopt linear, cyclic, or branched topologies, as documented by recent theoretical studies.[6−9] The hydrogen-bonded hydroxyl groups represent a backbone of the cluster, while the alkyl groups are the side chains (using the terminology of polymer chemistry).

Infrared (IR) spectroscopy is the most frequently used experimental method for studies of alcohol clusters. Murdoch et al.[10] presented a detailed study of dilute solutions of ethanol in three nonpolar solvents, *n*-hexane, CCl_4, and cyclopentane, employing IR spectroscopy, density functional theory (DFT)

Received: February 15, 2014
Revised: May 20, 2014
Published: May 22, 2014

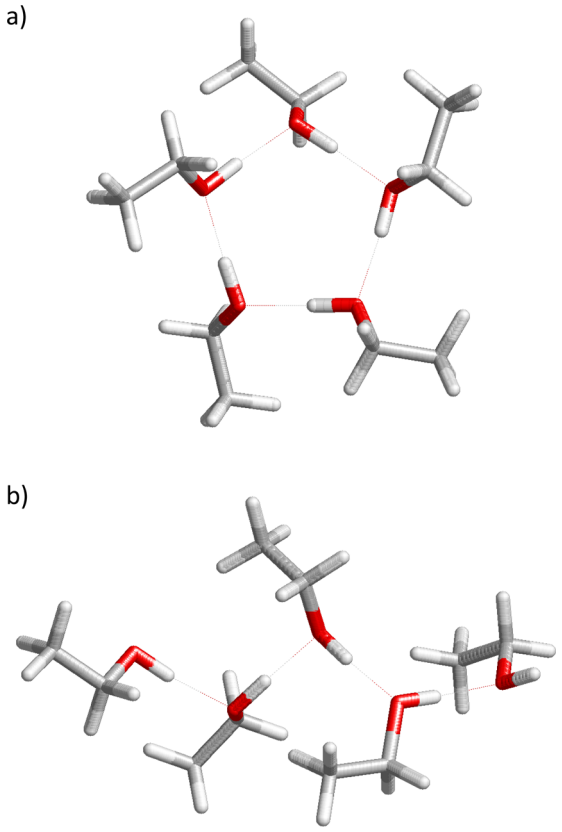

Figure 1. Examples of ethanol clusters: (a) cyclic and (b) linear pentamer consisting of monomeric units in the trans conformation.

calculations, and ^{1}H NMR chemical shifts analysis. Focusing mainly on the ethanol/*n*-hexane mixtures, they interpreted the temperature dependencies of three major IR bands in the O−H stretching region (3200−3700 cm^{-1}) in terms of populations of ethanol cluster of different sizes (i.e., of the monomer, cyclic tetramer, and cyclic pentamer/hexamer). The monomer was found to prevail at a temperature close to ambient, while the cyclic pentamer/hexamer dominated at low temperature (approximately 250 K and below, depending also on the concentration). Roughly 20% of ethanol molecules were estimated to form cyclic tetramers (with only a weak temperature dependence). By comparing different nonpolar solvents, they found that the population of ethanol monomer and small clusters in the ethanol/CCl_4 mixture was substantially larger than in the ethanol/*n*-hexane mixture at the same ethanol concentration. This clearly demonstrated different alcohol clustering properties in different nonpolar solvents. It was later shown that CCl_4 does not act as an "innocent" solvent for hydrogen-bonding liquids due to the stabilizing interaction between the atomic quadrupole of Cl and the partial negative charge of the hydrogen bond acceptor.[11] Murdoch et al. also calculated chemical shifts of different clusters at the B3LYP/6-31+G* level of theory, but the results were presented only as the population averages corresponding to various experimental conditions.[10]

It is interesting to note that Gaffney et al.[12] used a different assignment of IR bands in their very similarly looking spectra of methanol-*d* dissolved in CCl_4. Rather than speaking of clusters of different size, they discriminated between a free monomer, the OD group-accepting hydrogen bond only, the OD group donating hydrogen bond only, and the OD group acting as the simultaneous donor and acceptor. More recently, ATR-IR spectroscopic studies of methanol/*n*-hexane and hexan-1-ol/*n*-hexane mixtures revealed only very small amounts of the alcohol monomer at room temperature throughout the entire concentration range,[13,14] which is in contrast to the previous results by Murdoch et al.[10] Such a discrepancy between two very similar methods demonstrates the challenges and uncertainties in determining the hydrogen-bonding structure of the alcohol mixtures. Some other approaches for this purpose are clearly needed.

Liquid alcohols and their mixtures with nonpolar solvents have been extensively studied computationally. Early molecular dynamics (MD)[15−17] and Monte Carlo[18] studies of alcohols relying on classical pair-additive potentials suggested that the dominant hydrogen-bonded structures are large branched chains. Relatively rare events of cyclic cluster formation were calculated in higher alcohols[19] or in mixtures with nonpolar solvents at low alcohol concentrations.[20,21] The MD results are, however, contradicted by the experimental evidence as well as by quantum chemistry methods, which all point to the dominant population of small cyclic clusters at standard conditions.

There is a class of studies utilizing the X-ray or neutron diffraction possibly augmented with MD simulations. Sarkar and Joarder[22,23] suggested the cyclic hexamer as the dominant structure in neat liquid methanol and ethanol. Conversely, Yamaguchi et al.[24] proposed that neat methanol contains chain of average size of only 2.7 molecules even at 193 K. Another work addressing the size of the clusters in neat ethanol is that of Ferris and Farrar[25] who used a combination of the hydroxyl ^{1}H chemical shift with the ^{2}H (from ethanol-*d*) longitudinal relaxation time measurements along with quantum chemical calculations, and they proposed the cyclic pentamer as the major species in neat ethanol at ambient temperature.

More recently, Bloch and Lawrence[26] investigated hydrogen-bonded clusters of methanol in carbon tetrachloride. They employed MD simulations and compared the results with the rotational correlation times obtained previously by NMR.[27] Their study, however, suffers from an uncertainty in the size and topology of the clusters present at different concentrations. Two utilized calculation models provided very different populations of the cluster species classified as monomer, dimer, linear (including branched), and cyclic. Nevertheless, the rotational correlation time (obtainable also by the NMR relaxation) seemed to correspond to the hydrogen bond lifetime. A firm knowledge of the size of the present clusters is thus the major prerequisite for studying other properties such as the topology, bonding thermodynamics including effects of cooperativity, bond lifetimes, etc.

The hydrogen-bond lifetimes in the work of Bloch and Lawrence[26] were estimated to be on the order of picoseconds. This observation is consistent with the hydrogen bond breaking and reassociation times on the order of 1−10 ps (as obtained by the vibrational relaxation).[12,28,29] Given the fact that the fine details of internal structure such as the conformation of individual constituting units of the cluster and its topology strongly complicate the analysis of both the vibrational and NMR spectra and possibly cast doubts concerning some of the conclusions reviewed above, in this paper we propose a new method for a determination of the average ethanol cluster size. This method employs the NMR measurement of the self-diffusion coefficient. In order to correlate the experimental diffusion coefficient with a particular size of the clusters, we

dx.doi.org/10.1021/jp501648x | J. Phys. Chem. B 2014, 118, 6864−6874

make use of the hydrodynamic calculation performed using the HydroNMR program developed by Garcìa de la Torre.[30] For its application to small molecular species, we adjusted some of its settings through the independent calibration using dilute tetramethylsilane (TMS) solution in *n*-hexane. The cluster geometries for hydrodynamic modeling are generated by quantum chemical calculations.

II. THEORY

A. Diffusion. Molecules or generally any particles in liquids are subject to the translational diffusion, which is characterized by the self-diffusion coefficient, D. In accordance with the Stokes−Einstein equation (sometimes referred to as the Einstein−Sutherland equation),[31] the diffusion coefficient of a spherical particle with the hydrodynamic radius r_H, moving in a continuous fluid of the viscosity η is given by eq 1 (T is the absolute temperature and k_B is the Boltzmann constant).

$$D = \frac{k_B T}{6\pi\eta r_H} \tag{1}$$

Despite the assumptions made in the derivation of the Stokes−Einstein relationship, eq 1 is sometimes used to derive r_H from the diffusion coefficients for larger spherical molecules. However, it fails to predict the correct r_H for molecules with hydrodynamic radii comparable to those of the solvent molecules.

Several modifications of eq 1 were proposed, retaining a part of the original Stokes−Einstein approach, in order to make it valid for the small and possibly nonspherical molecules. Initially, it was proposed to change the factor of 6 (stick-boundary conditions) to 4 (slip-boundary conditions) in order to account for a missing solvation layer around most of the small molecules (see the work of Edward[32] and references therein).

Other authors suggested the modification of Stokes−Einstein equation in the form of

$$D = \frac{k_B T}{c\pi\eta r_H} \tag{2}$$

with the numerical factor c dependent on the ratio between the hydrodynamic radius of the solute (r_H) and the solvent (r_{solv}). An expression for c as a function of r_H and r_{solv} was derived by Gierer and Wirtz[33] and later empirically modified by Chen and Chen.[34] As discussed by Macchioni et al.,[35] the correction factors for the molecules with the hydrodynamic radii ranging from 3 to 6 Å are significantly smaller than 4, varying with the molecular size.

Yet another factor, f_s, must be included in the denominator of eq 2 when considering nonspherical molecules. For the ellipsoid-shaped molecules, a formula depending on the ratio between the major and minor semiaxes of the ellipsoid was introduced by Perin.[36]

III. MATERIALS AND METHODS

A. Samples. Three NMR samples were used in our work. TMS/*n*-hexane sample (for the adjustment of the HydroNMR parameters and for the use as a diffusion reference) was prepared in the coaxial NMR tube set (Shigemi) with the inner tube containing 1 vol % of the NMR standard tetramethylsilane (TMS) (Acros Organics, 99%) dissolved in approximately 400 μL of *n*-hexane (nondeuterated, Sigma-Aldrich, Reagent-Plus grade) and the outer tube containing deuterated methanol for the field-frequency lock. Two ethanol samples (for ethanol cluster size investigation) contained ethanol (MERCK, absolute grade for analysis) at the concentrations of 0.16 and 0.44 M dissolved in deuterated *n*-hexane-d_{14} (Armar Chemicals, 99.0% d). A small amount of the TMS standard was added to the ethanol samples. All the samples were degassed by the freeze−pump−thaw procedure performed several times and flame-sealed in the 5 mm NMR tube.

B. NMR Experiments. All NMR experiments were performed on Bruker Avance spectrometer with the resonance frequency for the proton nuclei of 500 MHz (11.7 T). For the translational diffusion measurements on ^{1}H nuclei, TBO, and TBI probes equipped with the gradient coils in the z axis were used. Variable temperature measurements were performed in the temperature range of 210−330 K with the step of approximately 10 K. The temperature calibration was done prior to the experiments using the standard methanol sample. The gradient strength was calibrated using Gd-doped water (D_2O + 1% H_2O) at 298 K, the maximum strength was 0.562 T m^{-1} at TBO and 0.553 T m^{-1} at TBI probehead.

The translational diffusion was measured on ^{1}H nuclei using the convection-compensated double-stimulated echo (DSTE) pulse sequence with bipolar gradients (similar to the sequence devised by Jerschow and Müller[37]) in order to minimize the possible effect of the flow due to the temperature gradient in the sample, especially at the lowest temperatures. A spin lock was used prior to the acquisition to get rid of some minor phase distortions in the spectra.[38] The number of scans was 16 with 2 dummy scans for the experiments on the TMS/*n*-hexane sample and 8 scans without dummy scans for the ethanol/TMS/*n*-hexane-d_{14} samples. The $\pi/2$ pulse length varied from 13.0 to 14.5 μs for the TBO probe and from 7.9 to 10.3 μs for the TBI probe throughout the measured temperature range. The values of the diffusion mixing time Δ (defined as a distance between the dephasing and rephasing gradient pulse, found twice in the DSTE sequence, $\Delta = T + 2\delta + 2\tau$ in the notation of Jerschow and Müller[37]) in both the TMS/*n*-hexane and ethanol/TMS/*n*-hexane-d_{14} measurements ranged from 80 ms (for the lowest temperature) to 15 ms (the highest temperature). The gradient pulses were half-sine-shaped, with δ = 2 ms duration of the whole bipolar pulse pair.

The series of one-dimensional (1D) spectra was recorded for 32 different values of the gradient strength linearly varied from 2 to 100% of the full gradient power. The values of the diffusion coefficients D were obtained by fitting the Gaussian decay function of a form suitable for the DSTE pulse sequence[37] (eq 3) to the signal intensity I versus the gradient strength g by a nonlinear least-squares regression using an in-house written Matlab routine. I_0 denotes intensity without applied gradient, γ_H is the gyromagnetic ratio of ^{1}H, g_{eff} is the effective gradient strength (i.e., $g_{eff} = 2g/\pi$ to account for the half-sine shape of the gradient pulse), and τ is the echo time.

$$I(g_{eff}) = I_0 \exp\left(-(\gamma_H g_{eff}\delta)^2\left[2\Delta - \frac{2}{3\delta} - \frac{\tau}{2}\right]D\right) \tag{3}$$

In principle, the expression in the square brackets of eq 3 is strictly valid only if the shape of the gradient pulses is rectangular.[39] However, according to our calculations performed using the strategy described by Price,[40] it differs from the correct form by an additive constant of $\delta/24$, which is negligible with respect to our Δ values.

dx.doi.org/10.1021/jp501648x | J. Phys. Chem. B 2014, 118, 6864−6874

All experiments were repeated at least twice at each temperature. The diffusion coefficients reported are the averages of at least two repeated measurements at each temperature and of several evaluated peaks for each species. The error estimates of the experimentally obtained diffusion coefficients are based on the Monte Carlo analysis of the fitted data and the statistics from multiple experiments. The possible sources of errors and the error propagation are discussed in Results and Discussion.

C. DFT Calculations. Geometries of ethanol clusters up to the octamer were optimized using the B3LYP functional[41,42] and the 6-31+G* basis set as implemented in Gaussian.[43] This level of theory has been used in previous computational studies due to its cost-effectiveness and an overall excellent performance for the hydrogen-bonded systems.[6−10] We considered only the ethanol clusters formed by the O···H−O hydrogen bonds, since the O···H−C bonds are much weaker.[5,8,44] The number of conceivable cluster topologies rapidly grows with the number of ethanol monomeric units. For the practical calculations up to the octamer, we considered the cyclic (C) and linear (L) clusters only. Moreover, we considered only the ethanol clusters with the monomers either all trans (T) or all gauche (G). Thus, the calculations were performed for two types of monomer (G and T), four types of dimer (GG, GT, TG, and TT), and four types of each cluster larger than the dimer: cyclic trans (TC), cyclic gauche (GC), linear trans (TL), and linear gauche (GL).

From the perspective of the hydrodynamic calculations, the cyclic and linear topologies represent two limiting cases: the most compact and the most elongated cluster types, respectively. Additionally, there is a possibility of forming a large number of the branched topologies involving the O−H···O···H−O link[6−9] that can be viewed as an intermediate case. Consequently, the branched topologies can be omitted for the purpose of this study. The similarity of the calculated hydrodynamic radii for all ethanol clusters with the same number of monomers (as documented in Figure 7, vide infra) justifies this choice.

The molecular structure of TMS needed for the adjustment of the HydroNMR parameter setting was calculated in the same way as were the ethanol clusters.

D. Hydrodynamic Simulations. The hydrodynamic simulations in this work were performed by the computer program HydroNMR,[30] which has been designed for the calculations of hydrodynamic properties and NMR quantities of small, quasi-rigid macromolecules. A detailed description of the program may be found in the literature,[45] here we limit ourselves to describe program's most important features.

The program is based on the bead modeling,[46,47] representing a real diffusing particle as an array of the spherical frictional particles: the beads. The program constructs a primary hydrodynamic model by replacing all nonhydrogen atoms with atomic spheres of a radius AER (atomic element radius). The primary hydrodynamic model is then used to derive the secondary shell model (a special case of the bead model), representing the surface of the particle by a large number of minibeads of the radius σ. The hydrodynamic calculation is carried out assuming that each minibead obeys the Stokes−Einstein law. The calculations are performed for several values of σ, ranging from σ_{max} to σ_{min}, and the result is taken from the extrapolation to the shell model limit of $\sigma \rightarrow 0$.

The input of the program contains the atomic coordinates of simulated species, the temperature, and the corresponding viscosity of solvent. Besides, a user also specifies the parameters of the shell model (i.e., AER, σ_{max}, and σ_{min}). In the performed simulations, the maximum and minimum radii of the minibeads, σ_{max} and σ_{min}, were fixed (dependent on the size of the simulated molecule) so that the minimum and the maximum numbers of minibeads were 600 and 2000 (current limit of the program), respectively.[45] The output from the HydroNMR contains the translational diffusion coefficient D of the studied molecule.

Two series of hydrodynamic calculations were performed. First, we sought to find optimal setting of the control parameter AER in order to correctly reproduce the translational diffusion of small molecules (as described in Results and Discussion, section A). The second series of the calculations concerned the total number of 28 ethanol cluster structures as obtained from the DFT calculations with the radii of the atomic spheres AER of 0.825 Å (as the result of the preceding optimization procedure), described in Results and Discussion, Section D.

IV. RESULTS AND DISCUSSION

A. Optimization of the HydroNMR Input Parameters. Hydrodynamic simulations of small entities (such as ethanol clusters) by HydroNMR require a special attention and prior investigation. In order to validate the use of HydroNMR for our purposes, we have chosen a model system of TMS dissolved in *n*-hexane, taking advantage of TMS being a symmetrical noninteracting molecule which does not participate in hydrogen bonding. Moreover, the size of TMS is comparable to the size of investigated ethanol molecular clusters. We sought to find the HydroNMR input settings, for which the predicted self-diffusion coefficients of TMS in *n*-hexane were consistent with those obtained from the NMR diffusometry experiments.

There are several adjustable parameters that control the run of the HydroNMR calculation.[45] From among them, we found that the setting of atomic element radius AER is critical for obtaining a good agreement between the calculation and experiment (we also investigated the influence of the minimal and maximal radius of the minibeads, σ_{min} and σ_{max}).

The experiments on TMS in *n*-hexane solution (TMS/*n*-hexane sample) were carried out in the temperature range of approximately 210−330 K, and the translational diffusion coefficients were evaluated for both TMS (D_{TMS}) and *n*-hexane (D_{hex}). The temperature dependence of D_{TMS} and D_{hex} values is presented in Figure 2.

The measured D_{hex} values are in good agreement with the values published by Harris[48] for the self-diffusion coefficient of the neat *n*-hexane, as shown in Figure 2, top part. Brüsewitz and Weiss[49] reported the diffusion coefficients of TMS/*n*-alkanes mixtures. Both D_{hex} and D_{TMS} are within the experimental error consistent with their data for the 0.1 molar fraction of TMS in *n*-hexane at the 0.1 MPa pressure (Figure 2). Our concentration of TMS was roughly 10-times lower, but the concentration dependence of the diffusion coefficients of the compounds is very weak, as shown in Brüsewitz's work.

The experimental values of diffusion coefficients of TMS and *n*-hexane suffer from relatively large error, estimated to be roughly 6%. The dominant source of the experimental error is due to the fact that the concentration of TMS has to be kept as low as possible, so that the viscosity of the solution would not deviate from the viscosity of the pure *n*-hexane. Thus, TMS diffusion coefficient is obtained by means of integration of a small peak close (by approximately 1 ppm) to a much larger

dx.doi.org/10.1021/jp501648x | J. Phys. Chem. B 2014, 118, 6864−6874

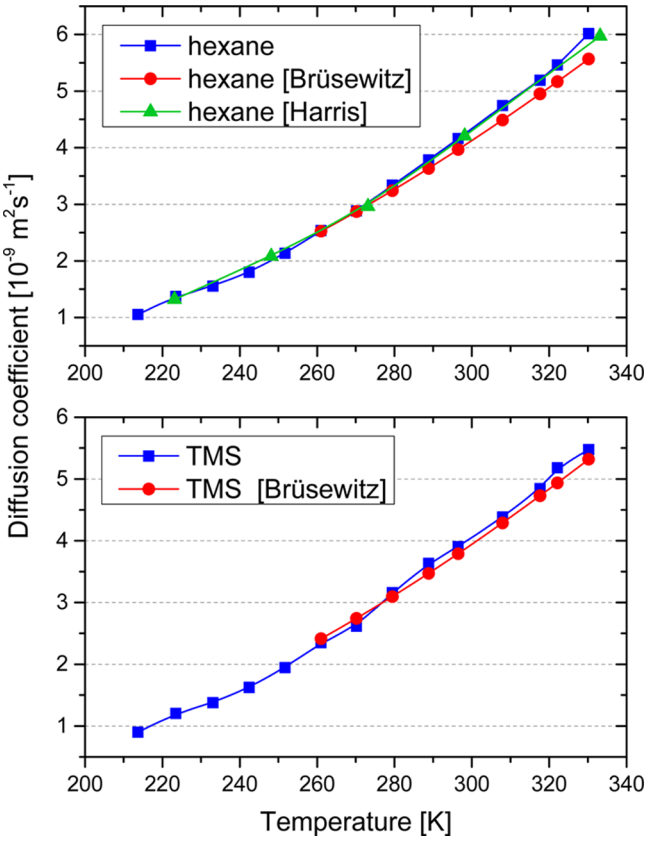

Figure 2. Temperature dependence of the experimental diffusion coefficients of *n*-hexane (top) and TMS (bottom) from the calibration experiments on TMS/*n*-hexane sample (blue ■), diffusion coefficients of neat *n*-hexane by Harris[48] (green ▲), diffusion coefficients of TMS, and *n*-hexane of 0.1 mole fraction TMS/*n*-hexane sample at 0.1 MPa pressure from Brüsewitz and Weiss[49] (red ●).

peak of *n*-hexane (at the natural isotopic abundance). Furthermore, the need for the ^{2}H field/frequency lock required a utilization of the coaxial tube set leading to broadening of the peaks in the spectrum.

Before we turn to the hydrodynamic simulations, it is important to comment on our way to correlate the diffusion properties obtained from experiments and simulations. The direct comparison of the temperature-dependent diffusion coefficients is rather inconvenient owing to the strong temperature dependence, imposed mostly by the temperature dependence of the solvent viscosity. We found it useful to multiply the diffusion coefficients by the solvent viscosity η and divide by temperature T to obtain a quantity which would reflect the (temperature-dependent) molecular size. This procedure is similar to the one used by Hedin et al.[50] to investigate the temperature-dependent micellar growth. Using the form of eq 2, we formally evaluate

$$cr_H = \frac{k_B T}{\pi \eta D} \tag{4}$$

which is freed from the explicit as well as the implicit (through η) temperature dependences. At this stage, for the purpose of comparison of the experimental and simulation data, we only assume that c is constant for TMS and *n*-hexane at all temperatures, without any further assumptions about its value.

We evaluated the cr_H products using eq 4 for TMS and hexane from the experimental D_{TMS} and D_{hex} values (the results

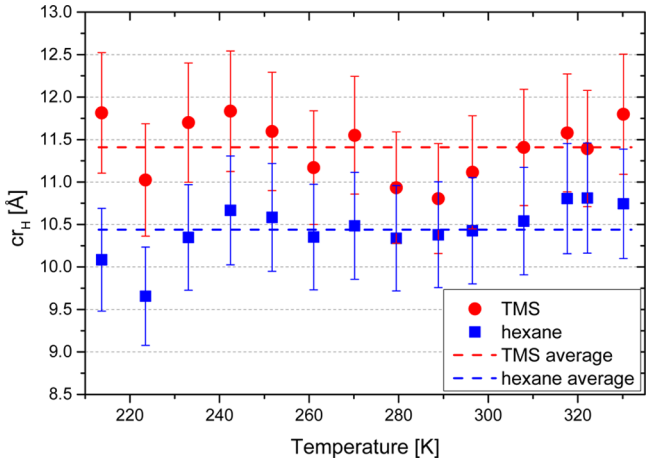

Figure 3. Values of cr_H for TMS (red ●) and *n*-hexane (blue ■), as calculated from the experimental diffusion coefficients according to eq 4 (TMS/*n*-hexane sample). The cr_H values are found to be independent of temperature, and the dashed lines show the corresponding average values for TMS (red line, 11.41 Å) and *n*-hexane (blue line, 10.44 Å).

are shown in Figure 3). The viscosity of TMS/*n*-hexane sample (η_{hex}) for this purpose was taken from Giller and Drickamer[51] as the viscosity of pure *n*-hexane, the influence of the dilute TMS was neglected. We performed the interpolation of their discrete data in order to obtain *n*-hexane viscosities at the temperatures of our experiments. Within the experimental error, cr_H appears to be temperature-independent for both TMS and hexane.

The hydrodynamic simulations on TMS in *n*-hexane were performed at two selected experimental temperature points, 296 and 260 K, with the corresponding viscosities obtained from the data of Giller and Drickamer,[51] as described above. The AER was varied by the steps of 0.005 Å in the range of 0.795−0.850 Å and by the steps of 0.001 in the range of 0.820−0.830 Å. The obtained diffusion coefficients were transformed into cr_H, according to eq 4. For AER value of 0.825 Å, the simulations in the whole experimental temperature range (approximately 210−330 K, step 10 K) were performed, confirming that the calculated cr_H values are, consistently with the experimental results, temperature independent (not shown). The cr_H values of TMS resulting from the simulations (taken as an average over the two temperatures of 296 and 260 K) are found to be linearly dependent on the set values of AER (Figure 3 and Table S2 of the Supporting Information). The cr_H versus AER dependence was fitted to a linear function, and the optimal AER = 0.825 Å was found as an intersection of the linear fit with the average experimental value of cr_H of TMS equal to 11.41 Å (see Figure 4). This value of AER was used for further simulations on ethanol.

In order to estimate the influence of the minibeads settings, the hydrodynamic simulations were performed by varying the σ_{min}, so that the maximum number of minibeads ranged from 1400 to 2000 and σ_{max}, so that the minimum number of minibeads ranged from 500 to 900, with the step of 100. For each combination of σ_{min} and σ_{max}, simulation was performed with AER = 0.8 Å at 180.8 K. The resulting values of diffusion coefficients differed from each other by less than 1%.

B. Measurements of Ethanol/TMS/*n*-Hexane-d_{14} Samples. ^{1}H NMR diffusion measurements on the ethanol/TMS/*n*-hexane-d_{14} samples with the ethanol concentration of 0.16

dx.doi.org/10.1021/jp501648x | J. Phys. Chem. B 2014, 118, 6864−6874

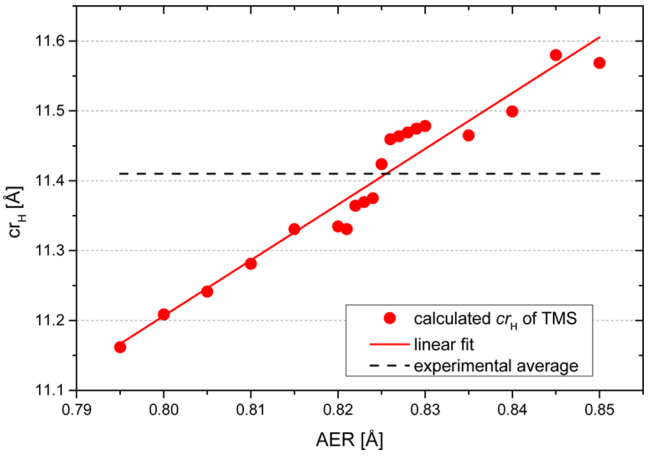

Figure 4. Procedure of optimization of the HydroNMR input value of the atomic sphere radius AER. Values of cr_H for TMS (red ●) as calculated by HydroNMR with varying settings of AER. The optimal setting of AER (0.825 Å) is found where the linear fit (red line) to the calculated data corresponds with the average cr_H of TMS (11.41 Å) obtained from the diffusion experiments on the TMS/*n*-hexane sample (black dashed line).

and 0.44 M were acquired in the temperature range of approximately 210−330 K; for selected ^{1}H spectra see Figure 5. In the ^{1}H spectra at ambient temperature (297 K), the chemical shifts of ethanol peaks are 3.58 ppm (CH_3), 1.15 ppm (CH_2), and 3.09 (OH, 0.16 M sample) or 4.32 ppm (OH, 0.44 M sample). Residual resonances of *n*-hexane are at 1.25 and 0.83 ppm. The resonance of TMS was used as the internal chemical shift standard. The chemical shift of the OH resonance is

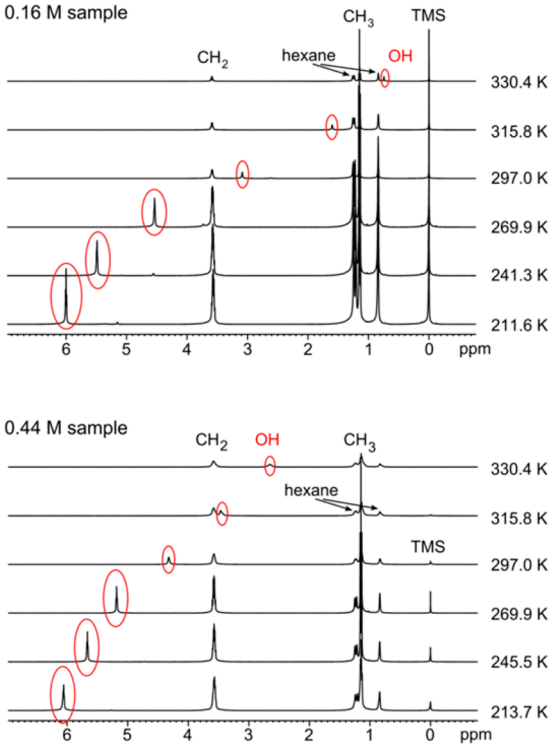

Figure 5. Temperature-dependent ^{1}H spectra of the ethanol/TMS/*n*-hexane-d_{14} samples with the ethanol concentration of 0.16 M (top) and 0.44 M (bottom). Temperature-dependent positions of OH group resonance are highlighted.

changing within the temperature range from 6.00 ppm (212 K) to 0.74 ppm (330 K) for the 0.16 M sample and from 6.06 ppm (214 K) to 2.65 ppm (330 K) for the 0.44 M sample (Figure 6). The temperature- and concentration-dependent OH

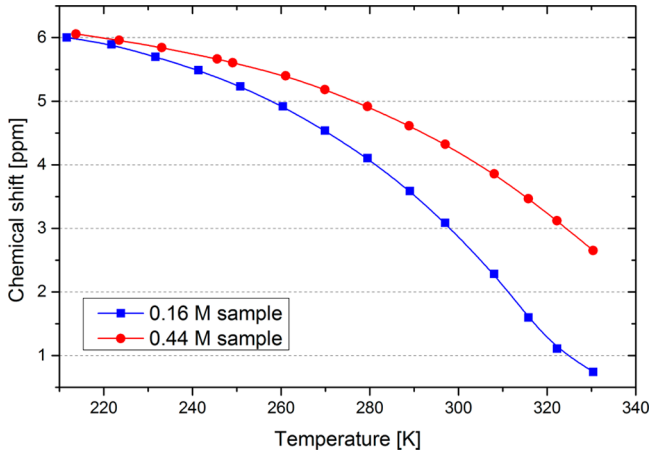

Figure 6. Temperature dependence of ^{1}H chemical shifts of the OH resonance for the ethanol/TMS/*n*-hexane-d_{14} samples with the ethanol concentration of 0.16 M (red ●) and 0.44 M (black ■).

chemical shift is connected to the hydrogen-bonding state of the OH group. The presence of a single resonance of the hydroxyl group (without any observable broadening), representing population-averaged contributions from the various hydrogen-bonding states of the OH group, means that even at the lowest temperature (210 K), the hydrogen-bonded clusters are in fast exchange between each other on the observed chemical shift timescale. Here, the difference between the highest and lowest OH chemical shifts is roughly $\Delta\omega \approx 6$ ppm, which indicates the exchange (i.e., cluster reorganization) occurring on the timescale much faster than $2/\Delta\omega \approx 700$ μs.

The chemical shift of the other ^{1}H signals is practically independent of the temperature (shifted by less than 0.02 ppm in the measured temperature range). The OH shift connection with the formation of the molecular clusters of ethanol is further discussed in Section E below.

The translational diffusion coefficients were evaluated separately for the OH and CH_2 resonances of ethanol, the CH_3 resonance of TMS, and the residual CH_3 resonance of deuterated *n*-hexane for both 0.16 and 0.44 M ethanol/TMS/*n*-hexane-d_{14} samples from the NMR diffusometry experiments using the procedure described in Materials and Methods, NMR Experiments. The ethanol CH_3 and *n*-hexane CH_2 signals were excluded from the analysis due to their spectral overlap. The obtained results are presented in Figure 7 and Table S3 of the Supporting Information. The single Gaussian decay of the signal intensity attenuation in the NMR diffusometry experiments is consistent with the timescale of the ethanol clusters' reorganization being much faster than the chemical shift timescale involved (as discussed above) as well as the timescale of the diffusion time Δ. This means that the measured diffusion coefficient is an average through all the cluster species at the given temperature and concentration, weighted by their relative populations.

It is evident from the inspection of Figure 7 that the diffusion coefficients of TMS (from the ethanol/TMS/*n*-hexane-d_{14} samples) are highly similar throughout the whole investigated temperature range for both samples that differ by the ethanol

dx.doi.org/10.1021/jp501648x | J. Phys. Chem. B 2014, 118, 6864−6874

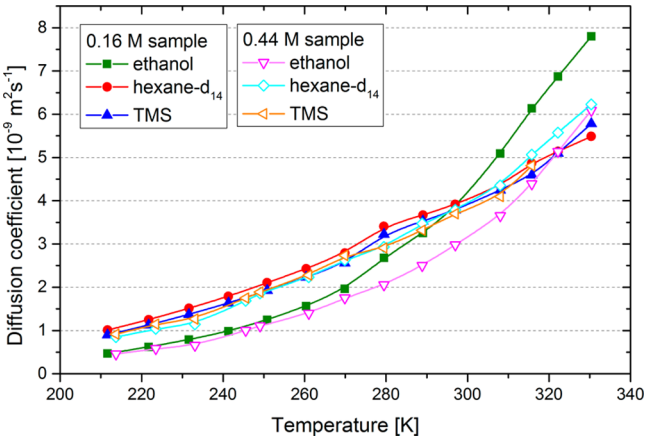

Figure 7. Temperature dependence of the experimental diffusion coefficients for all three compounds in the ethanol/TMS/*n*-hexane-d_{14} samples with the ethanol concentration of 0.16 and 0.44 M.

concentration (0.16 and 0.44 M). This holds also for the diffusion coefficients of the *n*-hexane-d_{14}. This observation is consistent with the assumption of a negligible difference in the viscosity between the two ethanol/TMS/*n*-hexane-d_{14} samples. On the contrary, the diffusion coefficients of ethanol display the temperature and concentration dependences different from those of TMS and *n*-hexane-d_{14}.

In analogy with the TMS/hexane experiment, we have chosen also in the case of the ethanol/TMS/*n*-hexane-d_{14} samples to eliminate the explicit as well as the implicit (i. e., that involved in the viscosity) temperature dependence by transforming the diffusion coefficients into the cr_H product values. Unlike for *n*-hexane, we are not aware of the viscosity data for the deuterated *n*-hexane-d_{14} in the investigated range of temperatures, and therefore, eq 4 cannot be used directly. Instead, in order to obtain the cr_H values from the experimental diffusion coefficients, we used the TMS as an internal diffusion standard (as described by Cabrita and Berger[52] or Macchioni et al.[35]). From eq 4, it follows that the $(cr_H)^{eth}$ of ethanol can be obtained from the $(cr_H)^{TMS}$ of TMS and the ratio of the diffusion coefficients of TMS ($D_{TMS}^{hex-d14}$) and ethanol ($D_{eth}^{hex-d14}$) in ethanol/TMS/*n*-hexane-d_{14} solution at a particular temperature, without the direct knowledge of the viscosity of the solution:

$$(cr_H)^{eth} = (cr_H)^{TMS} \frac{D_{TMS}^{hex-d14}}{D_{eth}^{hex-d14}} \quad (5)$$

The $(cr_H)^{TMS}$ = 11.41 Å was taken from the independent measurements of TMS in *n*-hexane (described in Results and Discussion, Optimization of the HydroNMR Input Parameters), assuming the same hydrodynamic radius of TMS in both solutions. This assumption is supported by similar values of the diffusion coefficients of TMS in both ethanol/TMS/*n*-hexane-d_{14} solutions. The same procedure was used to calculate the $(cr_H)^{hex}$ values from the diffusion coefficients of *n*-hexane-d_{14}.

Note that for the 0.44 M sample, the TMS resonance was not present at the two highest temperatures (322 and 330 K), which is ascribed to the evaporation of TMS to the free volume of the NMR tube due to its rather low boiling point (26–28 °C). As a consequence, it was not possible to perform the calculation of the $(cr_H)^{eth}$ value using eq 3 at these points. Instead, we used the fact that the $(cr_H)^{hex}$ of *n*-hexane-d_{14} shows no apparent temperature dependence (Figure S3 and Table S4 of the Supporting Information), and we calculated the missing points using eq 6.

$$(cr_H)^{eth} = (cr_H)^{hex} \frac{D_{hex-d14}}{D_{eth}} \quad (6)$$

For $(cr_H)^{hex}$, we took the value of 10.28 Å, which is the average value for *n*-hexane-d_{14} in the 0.44 M ethanol/TMS/*n*-hexane-d_{14} sample over the temperatures 210–315 K.

In contrast to the temperature-independent cr_H values for TMS or *n*-hexane-d_{14}, the obtained $(cr_H)^{eth}$ values of ethanol are, confirming the expectations, temperature-dependent, ranging from approximately 23 Å at the lowest temperature (213 K) to 11 Å at 330 K for the 0.44 M sample and reaching the plateau of 8.5 Å at above 308 K for the 0.16 M sample (Figure 8 and Figure S3 and Table S4 of the Supporting Information).

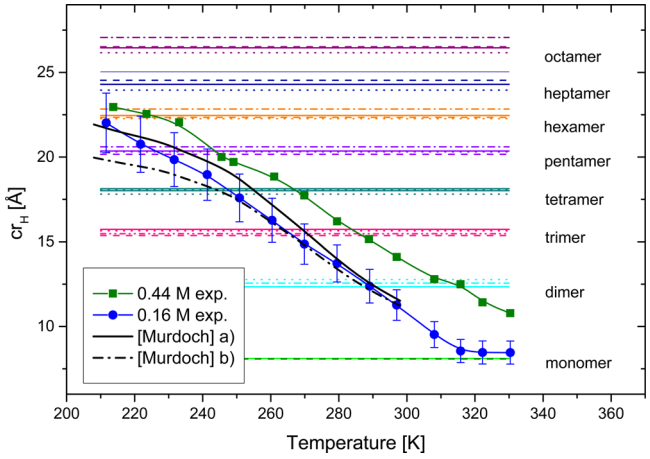

Figure 8. Temperature dependence of cr_H values of ethanol clusters in ethanol/TMS/*n*-hexane-d_{14} solutions. Horizontal straight lines are the theoretical values for the clusters of indicated sizes (monomer–octamer). Different types of lines of the same color correspond to different types of clusters (GC, solid; GL, dashed; TC, dotted; TL, dash-dotted). The experimentally determined cr_H values from 0.44 M (green ■) and 0.16 M (blue ●) are compared with the values derived from populations reported by Murdoch et al.[10] based on (a) monomer–tetramer–pentamer (black solid line) and (b) monomer–tetramer–hexamer equilibria (black dash-dotted line).

C. Calculated Geometries of Ethanol Clusters. Stable energy minima were found for ethanol clusters of all types and sizes, as was confirmed by the vibrational analysis performed for the optimized structures. The hydrogen-bonding geometry parameters are summarized in Figures S1 and S2 of the Supporting Information.

Clearly, the hydrogen bonding in the cyclic clusters is tighter than in the linear clusters of the same size, as documented by the approximately 0.01–0.02 Å difference in the R(O···O) distances between the two cluster types (Figure S1 of the Supporting Information). Further, the hydrogen bonds are usually slightly shorter in the clusters consisting of the gauche monomers. The average hydrogen bond length in the cyclic clusters systematically decreases with the increasing cluster size. The limiting values R(O···O) = 2.726 Å for GC and 2.736 Å for TC clusters are reached already for the hexamer. In contrast, the hydrogen bond lengths in the linear clusters are slightly but steadily decreasing even for the octamer.

dx.doi.org/10.1021/jp501648x | J. Phys. Chem. B 2014, 118, 6864–6874

The terminal hydrogen bonds in the linear clusters are significantly longer than the internal hydrogen bonds (Figure S1 of the Supporting Information). This is mainly caused by the absence of solvent in our calculations. Reliable solvent modeling for extended hydrogen-bonded systems is still a challenging task. However, such an effort was not necessary in our case since the hydrodynamic simulations are not overly sensitive to subtle geometry changes. The only exception might be the dimer, whose hydrogen bond length may be somewhat overestimated and, consequently, the calculated diffusion coefficient might be slightly underestimated.

The A(O−H···O) values for the cyclic trimer close to 150° imply serious deviations of the hydrogen-bonding geometry from the ideal linear case (Figure S2 of the Supporting Information). Indeed, the hydrogen bonds in three-membered rings have been previously found less stable than those in the larger cyclic clusters.[8,9,53] Also the current interpretation of spectroscopic measurements does not indicate any significant population of cyclic trimers.[10] The hydrogen-bonding geometry in the cyclic tetramers with the A(O−H···O) values below 170° is also not ideal, but the hydrogen bonds are already quite strong,[8,9,53] and the existence of these and larger clusters has been experimentally confirmed.[10,25]

D. Hydrodynamic Simulation of Ethanol Clusters. Hydrodynamic calculations were carried out separately for each size of the cluster (from the monomer to octamer) and for each structure type (GC, GL, TC, TL, as described in Materials and Methods, Hydrodynamic Simulations) at the temperature range corresponding to the experiments.

The ethanol/TMS/*n*-hexane-d_{14} samples with ethanol concentration of both 0.16 and 0.44 M were sufficiently diluted, and thus we neglected a possible difference in viscosities between the two samples. As already stated, we are not aware of the viscosity data for the deuterated *n*-hexane in the investigated range of temperatures. As an input to the hydrodynamic simulations, the temperature-dependent viscosities of the deuterated *n*-hexane-d_{14} were calculated from the values for *n*-hexane as $\eta_{\mathrm{hex}-d14} = (M_r)^{1/2}\eta_{\mathrm{hex}}$, where M_r is the molecular mass ratio (M_r = 1.16 for *n*-hexane-d_{14}/*n*-hexane). In accordance with Holz and co-workers,[54] this approximation is reasonable for linear alkanes.

The cr_H values for each type of ethanol cluster were evaluated from the diffusion coefficients obtained by the HydroNMR simulations according to eq 4. The resulting cr_H values, for a given type of cluster, are found temperature-independent. This fact is not surprising, since we expect the hydrodynamic radius r_H to be temperature-independent for each type of cluster. The cr_H values were averaged over the whole temperature range for each type of ethanol clusters and are reported in Table 1.

The calculated data show that the diffusion properties of the ethanol clusters of the same size are not influenced by the rotameric state of the constituting monomeric units. The clusters consisting of the gauche units display the same diffusion coefficients as those consisting of the monomers in the trans conformation (Table 1 and Figure 8).

Furthermore, the differences in the diffusion coefficients between the cyclic and the linear clusters were increasing with the size of the clusters, reaching up to 4% (Table 1 and Figure 8). These differences are ascribed to the fact that the larger clusters deviate from the spherical shape more than the smaller ones. This observation is consistent with that of Macchioni et al.,[35] who found that a significant deviation of the diffusion coefficient due to the nonspherical shape of the molecules is encountered when the semiaxes ratio of the molecular ellipsoid is greater than 3. From the direct measurements of the interatomic distances along the short and long axes of the DFT calculated cluster structures (not shown), this is not the case for any of the cyclic clusters nor for the linear clusters up to the size of the heptamer.

Table 1. Values of cr_H Averaged over the Whole Temperature Range of Theoretical Ethanol Cluster Structures from Monomer to Octamer As Obtained from the HydroNMR Hydrodynamic Simulations (G, gauche; T, trans; C, cyclic; L, linear)

	cr_H (Å)			
	G	T		
monomer	8.11	8.08		
	GG	GT	TG	TT
dimer	12.34	12.34	12.77	12.56
	GC	GL	TC	TL
trimer	15.73	15.37	15.65	15.48
tetramer	18.02	17.81	18.06	18.13
pentamer	20.36	20.17	20.31	20.61
hexamer	22.46	22.35	22.27	22.84
heptamer	24.30	24.54	23.96	25.04
octamer	26.46	26.52	26.17	27.06

Thus, the theoretically determined diffusion coefficients depend mainly on the sizes of the clusters, while the fine details of the cluster structure topology make only marginal contribution. This feature underlines a usefulness of the diffusion coefficients for an analysis of alcohol clusters.

E. Average Size of Ethanol Molecular Clusters. The correlation of the calculated and experimental hydrodynamic properties of ethanol allows us to relate the diffusion coefficients from the experiment to the actual number of ethanol molecules within the clusters (i.e., to the average size of the clusters). The comparison between the diffusion coefficients of ethanol with the same quantities obtained from the HydroNMR simulations of the DFT-calculated ethanol clusters is facilitated by the transformation of D into the cr_H values (to eliminate an influence of the solvent viscosity and temperature), according to eq 4. The results are reported in Figure 8.

Note that from the hydrodynamic simulations we obtain the diffusion coefficient for a certain type and size of ethanol clusters, whereas the diffusion coefficient resulting from the experiments at a certain temperature and ethanol concentration is an arithmetic mean of the diffusion coefficients of the various clusters present, weighted by their relative populations. By inspecting eq 4, it follows that a similar relationship is valid for cr_H. The cr_H value obtained from the experiment is a weighted harmonic mean of the cr_H values of all the clusters present. Moreover, cr_H reflects the sizes of the diffusing particles, therefore by comparison of the values obtained from experiments with those from the calculations we obtain the temperature and concentration dependence of the average size of the ethanol clusters.

The average size of the clusters in 0.44 M sample is systematically somewhat larger than in the 0.16 M sample, roughly by one ethanol unit. At low temperatures cr_H values for the 0.16 M ethanol samples correspond to the pentamer−hexamer, and those of 0.44 M ethanol samples correspond to an average cluster size of the hexamer. At the temperatures

dx.doi.org/10.1021/jp501648x | J. Phys. Chem. B 2014, 118, 6864−6874

higher than 300 K, the clusters of average size close to a dimer are present in the 0.44 M sample. In contrast, monomers are significantly populated above this temperature in the 0.16 M sample. This experimental observation of a lower bound of the size of the ethanol clusters is in excellent agreement with the cr_H value predicted for the ethanol monomer by hydrodynamic calculations. This fact validates the employed methodology and reinforces our interpretation of the diffusion NMR data.

Furthermore, the OH chemical shifts of ethanol (Figure 6) provide an independent semiquantitative measure of the size of the present clusters at high temperatures when only small clusters (monomer, dimer, etc.) are populated. The relation of the chemical shift to the size of the present clusters is, however, much less straightforward than that of the diffusion coefficient. Considering the chemical shift, there are, in principle, two main types of OH groups in the oligomer backbone: hydrogen donors (including the inner OH groups that act as simultaneous donors and acceptors) and the exclusive hydrogen acceptors (terminal groups in the linear clusters) with their own hydrogen not being involved in hydrogen bonding. The donor OH groups dominate at low temperatures when large and possibly cyclic clusters are populated. Thus, the chemical shift of the donor OH group can be estimated as roughly 7 ppm according to the low temperature spectrum (considering 5 donors and possibly 1 exclusive acceptor OH in the hexamer, on average) (Figure 6). Conversely, the upper bound of the chemical shift of the terminal exclusive acceptor OH group can be determined as 0.7 ppm from the spectrum of 0.16 M sample at 330 K, in which only the monomer is present. In this way, the presence of the average dimer (based on the diffusion measurement) can be verified by the value of the chemical shift. The OH chemical shifts in the spectra of the 0.16 M sample at 289 K and 0.44 M sample at 315.8 K are indeed close to 3.2 ppm, which is the estimated value of the average OH shift in the dimer.

The error of determination of the cr_H values (by eq 5) for ethanol, as depicted by the error bars in Figure 8, stems from two major additive contributions. The first contribution is from the average $(cr_H)^{TMS}$ of TMS obtained from the TMS/*n*-hexane experiments, as discussed above. The second source of error comes from the ethanol and TMS diffusion coefficient (experiments on ethanol/TMS/*n*-hexane-d_{14} samples), and it is estimated here to contribute by 4 relative percent. The total experimental error can be also estimated by a random fluctuation of the temperature dependence of cr_H of *n*-hexane-d_{14} (Figure S4 and Table S4 of the Supporting Information). The standard deviations from the average cr_H value of *n*-hexane-d_{14} over temperatures are 5% and 3% for the 0.16 and 0.44 M samples, respectively, which compares well with the error estimated for ethanol.

The scatter in the theoretically predicted diffusion coefficients is clearly smaller than the experimental error. We believe that the adopted adjustment procedure utilizing the average hydrodynamic radius of TMS from 14 temperature-dependent measurements of dilute TMS in *n*-hexane (Figure 2) greatly reduces the possible error.

The early works on hydrogen bonding in ethanol and related low-molecular alcohols were usually limited to analyses of chemical shift[4,55] or relaxation rates,[56] typically at room temperature. Nevertheless, the findings of Saunders and Hyne[4] considering the models of monomer−tetramer, monomer−trimer, or monomer−dimer equilibria at room temperature are not in contradiction with our results. Using the novel experimental and theoretical tools, such as the NMR diffusometry, the accurate variable temperature control, and the quantum chemical DFT calculations, we obtained quantitative data in a much wider range of temperatures.

A comparison of our results with the ethanol cluster types predicted by Murdoch et al.[10] was included in Figure 8. We extracted the cluster populations (monomer, tetramer, and pentamer/hexamer) reported for 2 mol % ethanol in *n*-hexane (which corresponds to the 0.16 M molar concentration) and calculated the corresponding averaged cr_H values employing our theoretical cr_H values of the different clusters (Table 1). Murdoch et al. assigned the IR band corresponding to "large" clusters ambiguously to the pentamer/hexamer. The two curves in Figure 8, therefore, correspond to the two limit cases that the "large" clusters are represented solely by the pentamer or by the hexamer. The agreement of our results with those of Murdoch et al. is very good; our curve lies within the range of the two curves based on the work of Murdoch et al., being closer to the pentamer model at higher temperatures while getting close to the hexamer model at low temperatures.

For the 0.44 M sample, we observed a partial saturation of the growth of the cluster sizes toward low temperature (Figure 8). Further, the cluster size also grew with increasing ethanol concentration, which persisted even at the lowest temperatures. This behavior suggests that it is a kinetic effect of hydrogen bond lifetime competing with the probability of a collision leading to a formation of larger clusters that impose an effective limit to the size of ethanol clusters at low temperature. This hypothesis however requires some more detailed concentration- and temperature-dependence studies.

V. CONCLUSIONS

In this paper, we have described a novel method for the hydrogen-bonding investigation that combines the measurements of diffusion coefficient performed by means of NMR diffusometry technique and the hydrodynamic simulations. This approach includes the use of the HydroNMR program for small molecules, which is facilitated here by the calibration procedure using the dilute solution of tetramethylsilane. It is thus possible to correlate the experimentally determined diffusion coefficients converted to the cr_H values of ethanol with the same quantities of the modeled ethanol clusters of different sizes.

Specifically, we investigated two dilute solutions of ethanol in deuterated *n*-hexane (0.16 and 0.44 M) at large temperature range approximately 210−330 K. The size of ethanol clusters (i.e., the number of the ethanol units) as obtained from the diffusion measurements combined with the hydrodynamic simulations generally decreases with increasing temperature. This trend stops at temperatures above 300 K for the more dilute sample (0.16 M), where the cr_H remains constant, equal to the value calculated for the ethanol monomeric species. This agreement between the experiment and simulation provides also a verification of the presented methodology. At low temperatures, the average size of the present clusters corresponds roughly to the pentamer or the hexamer. The 0.44 M solution is composed of somewhat larger clusters in the whole temperature range with the average cluster sizes ranging roughly from the dimer to the hexamer.

The methodology presented in this paper enlarges the portfolio of methods useful for elucidation of the structure and the cluster composition of dilute mixtures of alcohol in the liquid state. The major advantage of our new method is the

dx.doi.org/10.1021/jp501648x | J. Phys. Chem. B 2014, 118, 6864−6874

direct relation of the measured observable, the diffusion coefficient, to the size of the investigated clusters. Such one-to-one relation is not present in the methodologies most frequently used so far for the studies of hydrogen-bonded liquids.

■ ASSOCIATED CONTENT

Supporting Information

The hydrogen-bonding geometry parameters are summarized in Figure S1 [R(O···O) distances] and Figure S2 [A(O−H···O) angles]. Temperature-dependent diffusion coefficients of TMS and *n*-hexane and corresponding cr_H values from the experiments on TMS/*n*-hexane sample are listed in Table S1. Diffusion coefficients, cr_H values, and the corresponding input parameter settings from HydroNMR simulations on TMS/*n*-hexane for HydroNMR optimization are listed in Table S2. The experimental temperature-dependent diffusion coefficients of ethanol, *n*-hexane-d_{14}, and TMS in the ethanol/TMS/*n*-hexane-d_{14} samples with the ethanol concentration of 0.16 and 0.44 M are listed in Table S3. The corresponding cr_H values are plotted in Figure S3 and listed in Table S4. The data from HydroNMR simulations of ethanol in *n*-hexane-d_{14} are in Tables S5a−S5e. This material is available free of charge via the Internet at http://pubs.acs.org.

■ AUTHOR INFORMATION

Corresponding Author

*E-mail: jan.lang@mff.cuni.cz. Tel: +420 221 912 889.

Notes

The authors declare no competing financial interest.

■ ACKNOWLEDGMENTS

This research was supported by the Czech Science Foundation Grant P204/11/1206. Computational resources were partially provided under the programme "Projects of Large Infrastructure for Research, Development, and Innovations" LM2010005.

■ REFERENCES

(1) Suhm, M. A. Hydrogen Bond Dynamics in Alcohol Clusters. *Adv. Chem. Phys.* **2008**, *142*.

(2) Liddel, U.; Ramsey, N. F. Temperature Dependent Magnetic Shielding in Ethyl Alcohol. *J. Chem. Phys.* **1951**, *19*, 1608.

(3) Arnold, J. T.; Packard, M. E. Variations in Absolute Chemical Shift of Nuclear Induction Signals of Hydroxyl Groups of Methyl and Ethyl Alcohol. *J. Chem. Phys.* **1951**, *19*, 1608−1609.

(4) Saunders, M.; Hyne, J. B. Study of Hydrogen Bonding in Systems of Hydroxylic Compounds in Carbon Tetrachloride through the Use of NMR. *J. Chem. Phys.* **1958**, *29*, 1319−1323.

(5) Dyczmons, V. Dimers of Ethanol. *J. Phys. Chem. A* **2004**, *108*, 2080−2086.

(6) Boyd, S. L.; Boyd, R. J. A Density Functional Study of Methanol Clusters. *J. Chem. Theory Comput.* **2007**, *3*, 54−61.

(7) Mejía, S. M.; Espinal, J. F.; Restrepo, A.; Mondragón, F. Molecular Interaction of $(Ethanol)_2$-Water Heterodimers. *J. Phys. Chem. A* **2007**, *111*, 8250−8256.

(8) Mejía, S. M.; Espinal, J. F.; Mondragón, F. Cooperative Effects on the Structure and Stability of $(Ethanol)_3$−Water, $(Methanol)_3$−Water Heterotetramers and $(Ethanol)_4$, $(Methanol)_4$ Tetramers. *J. Mol. Struct.: THEOCHEM* **2009**, *901*, 186−193.

(9) David, J.; Guerra, D.; Restrepo, A. Structural Characterization of the $(Methanol)_4$ Potential Energy Surface. *J. Phys. Chem. A* **2009**, *113*, 10167−10173.

(10) Murdoch, K. M.; Ferris, T. D.; Wright, J. C.; Farrar, T. C. Infrared Spectroscopy of Ethanol Clusters in Ethanol-Hexane Binary Solutions. *J. Chem. Phys.* **2002**, *116*, 5717−5724.

(11) Torii, H. Atomic Quadrupolar Effect in the Methanol−CCl_4 and Water−CCl_4 Intermolecular Interactions. *Chem. Phys. Lett.* **2004**, *393*, 153−158.

(12) Gaffney, K. J.; Piletic, I. R.; Fayer, M. D. Orientational Relaxation and Vibrational Excitation Transfer in Methanol-Carbon Tetrachloride Solutions. *J. Chem. Phys.* **2003**, *118*, 2270−2278.

(13) Max, J.-J.; Chapados, C. Infrared Spectroscopy of Methanol-Hexane Liquid Mixtures. I. Free OH Present in Minute Quantities. *J. Chem. Phys.* **2008**, *128*, 224512.

(14) Max, J.-J.; Chapados, C. Infrared Spectroscopy of Methanol-Hexane Liquid Mixtures. II. The Strength of Hydrogen Bonding. *J. Chem. Phys.* **2009**, *130*, 124513.

(15) Jorgenssen, W. L. Structure and Properties of Liquid Methanol. *J. Am. Chem. Soc.* **1980**, *102*, 543−549.

(16) Haughney, M.; Ferrario, M.; McDonaldt, I. R. Molecular-Dynamics Simulation of Liquid Methanol. *J. Phys. Chem.* **1987**, *91*, 4934−4940.

(17) Matsumoto, M.; Hubbinds, K. E. Hydrogen Bonding in Liquid Methanol. *J. Chem. Phys.* **1990**, *93*, 1981−1994.

(18) Chen, B.; Potoff, J. J.; Siepmann, J. I. Monte Carlo Calculations for Alcohols and Their Mixtures with Alkanes. Transferable Potentials for Phase Equilibria. 5. United-Atom Description of Primary, Secondary, and Tertiary Alcohols. *J. Phys. Chem. B* **2001**, *105*, 3093−3104.

(19) Perera, A.; Sokolić, F.; Zoranić, L. Microstructure of Neat Alcohols. *Phys. Rew. E* **2007**, *75*, 060502.

(20) Veldhuizen, R.; Leeuw, S. W. Molecular Dynamics Study of the Thermodynamic and Structural Properties of Methanol and Polarizable/Non-Polarizable Carbon Tetrachloride Mixtures. *J. Chem. Phys.* **1996**, *105*, 2828−2836.

(21) Munaò, G.; Costa, D.; Saija, F.; Caccamo, C. Simulation and Reference Interaction Site Model Theory of Methanol and Carbon Tetrachloride Mixtures. *J. Chem. Phys.* **2010**, *132*, 084506.

(22) Sarkar, S.; Joarder, R. N. Molecular Clusters and Correlations in Liquid Methanol at Room Tempearuture. *J. Chem. Phys.* **1993**, *99*, 2032−2039.

(23) Sarkar, S.; Joarder, R. N. Molecular Clusters in Liquid Ethanol at Room Tempearuture. *J. Chem. Phys.* **1994**, *100*, 5118−5122.

(24) Yamaguchi, T.; Hidaka, K.; Soper, A. K. The Structure of Liquid Methanol Revisited: A Neutron Diffraction Experiment at −80 °C and +25 °C. *Mol. Phys.* **1999**, *96*, 1159−1168.

(25) Ferris, T. D.; Farrar, T. C. The Temperature Dependence of the Hydroxyl Deuterium Quadrupole Coupling Parameter and the Rotational Correlation Time of the OD Internuclear Vector in Neat Ethanol-d_1. *Mol. Phys.* **2002**, *100*, 303−309.

(26) Bloch, K.; Lawrence, C. P. Hydrogen Bond Lifetimes and Clustering of Methanol in Carbon Tetrachloride Solutions. *J. Phys. Chem. B* **2010**, *114*, 293−297.

(27) Wendt, M. A.; Farrar, T. C. An Indirect Method for the Measurement of Deuterium Quadrupole Coupling Constants in Liquids. *Mol. Phys.* **1998**, *95*, 1077−1081.

(28) Levinger, N. E.; Davis, P. H.; Fayer, M. D. Vibrational Relaxation of the Free Terminal Hydroxyl Stretch in Methanol Oligomers: Indirect Pathway to Hydrogen Bond Breaking. *J. Chem. Phys.* **2001**, *115*, 9352−9360.

(29) Graener, H.; Ye, T. Q.; Laubereau, A. Ultrafast Dynamics of Hydrogen Bonds Directly Observed by Timeresolved Infrared Spectroscopy. *J. Chem. Phys.* **1989**, *90*, 3413−3416.

(30) Garcìa de la Torre, J.; Huertas, M. L.; Carrasco, B. HYDONMR: Prediction of NMR Relaxation of Globular Proteins from Atomic-Level Structures and Hydrodynamic Calculations. *J. Magn. Reson.* **2000**, *147*, 138−146.

(31) Price, W. S. *NMR Studies of Translational Motion*; Cambridge University Press: Cambridge, U.K., 2009.

(32) Edward, J. T. Molecular Volumes and the Stokes-Einstein Equation. *J. Chem. Educ.* **1970**, *47*, 261−270.

(33) Gierer, A.; Wirtz, K. Molekulare Theorie der Mikroreibung. *Z. Naturforsch.* **1953**, *8*, 532−538.
(34) Chen, H.-C.; Chen, S.-H. Diffusion of Crown Ethers. *J. Phys. Chem.* **1984**, *88*, 5118−5121.
(35) Macchioni, A.; Ciancaleoni, G.; Zuccaccia, C.; Zuccaccia, D. Determining Accurate Molecular Sizes in Solution through NMR Diffusion Spectroscopy. *Chem. Soc. Rev.* **2008**, *37*, 479−489.
(36) Perrin, F. Mouvement Brownien d'un ellipsoide (II). Rotation libre et dépolarisation des fluorescences. Translation et diffusion de molécules ellipsoidales. *J. Phys. Radium* **1936**, *7*, 1−11.
(37) Jerschow, A.; Müller, N. Suppression of Convection Artifacts in Stimulated-Echo Diffusion Experiments. Double-Stimulated-Echo Experiments. *J. Magn. Reson.* **1997**, *125*, 372−375.
(38) Pelta, M. D.; Barjat, H.; Morris, G. A.; Davis, A. L.; Hammond, S. J. Pulse Sequences for High-Resolution Diffusion-Ordered Spectroscopy (HR-DOSY). *Magn. Reson. Chem.* **1998**, *36*, 706−714.
(39) Price, W. S.; Hayamizu, K.; Ide, H.; Arata, Y. Strategies for Diagnosing and Alleviating Artifactual Attenuation Associated with Large Gradient Pulses in PGSE NMR Diffusion Measurements. *J. Magn. Reson.* **1999**, *139*, 205−212.
(40) Price, W. S. Pulsed-Field Gradient Nuclear Magnetic Resonance as a Tool for Studying Translational Diffusion: Part I. Basic Theory. *Concepts Magn. Reson.* **1997**, *9*, 299−336.
(41) Becke, A. D. Density-Functional Thermochemistry. III. The Role of Exact Exchange. *J. Chem. Phys.* **1993**, *98*, 5648−5652.
(42) Stephens, P. J.; Devlin, F. J.; Chabalowski, C. F.; Frisch, M. J. Ab Initio Calculation of Vibrational Absorption and Circular Dichroism Spectra Using Density Functional Force Fields. *J. Phys. Chem.* **1994**, *98*, 11623−11627.
(43) Frisch, M. J;. Trucks, G. W; Schlegel, H. B.; Scuseria, G. E.; Robb, M. A.; Cheeseman, J. R.; Zakrzewski, V. G.; Montgomery, J. A., Jr.; Stratmann, R. E; Burant, J. C. et al. *Gaussian 98*, revision A.9; Gaussian, Inc.: Pittsburgh PA, 1998.
(44) Keefe, C. D.; Gillis, E. A. L.; MacDonald, L. Improper Hydrogen-Bonding CH·Y Interactions in Binary Methanol Systems As Studied by FTIR and Raman Spectroscopy. *J. Phys. Chem. A* **2009**, *113*, 2544−2550.
(45) Carrasco, B.; Garcìa de la Torre, J. Hydrodynamic Properties of Rigid Particles: Comparison of Different Modeling and Computational Procedures. *Biophys. J.* **1999**, *75*, 3044−3057.
(46) Bloomfield, V.; Dalton, W. O.; Van Holde, K. E. Frictional Coefficients of Multisubunit Structures. I. Theory. *Biopolymers* **1967**, *5*, 135−148.
(47) Bloomfield, V.; Dalton, W. O.; Van Holde, K. E. Frictional Coefficients of Multisubunit Structures. II. Application to Proteins and Viruses. *Biopolymers* **1967**, *5*, 149−159.
(48) Harris, K. R. Temperature and Density Dependence of the Self-Diffusion Coefficient of n-Hexane from 223 to 333 K and up to 400 MPa. *J. Chem. Soc., Faraday Trans. 1* **1982**, *78*, 2265−2274.
(49) Brüsewitz, M.; Weiss, A. Dependence of Mass Density and Selfdiffusion in Liquid Binary Systems n-Alkane/Tetramethylsilane on Temperature and Pressure. *Berichte der Bunsengesellschaft für Physikalische Chemie* **1993**, *97*, 1−9.
(50) Hedin, N.; Yu, T. Y.; Furó, I. Growth of $C_{12}E_8$ Micelles with Increasing Temperature. A Convection-Compensated PGSE NMR Study. *Langmuir* **2000**, *16*, 7548−7550.
(51) Giller, E. B.; Drickamer, H. G. Viscosity of Normal Paraffins near the Freezing Point. *Ind. Eng. Chem.* **1949**, *41*, 2067−2069.
(52) Cabrita, E. J.; Berger, S. DOSY Studies of Hydrogen Bond Association: Tetramethylsilane as a Reference Compound for Diffusion Studies. *Magn. Reson. Chem.* **2001**, *39*, 142−148.
(53) Ludwig, R.; Weinhold, F.; Farrar, T. C. Quantum Cluster Equilibrium Theory of Liquids: Molecular Clusters and Thermodynamics of Liquid Ethanol. *Mol. Phys.* **1999**, *97*, 465−477.
(54) Holz, M.; Mao, X.; Seiferling, D. Experimental Study of Dynamic Isotope Effects in Molecular Liquids: Detection of Translation-Rotation Coupling. *J. Chem. Phys.* **1996**, *104*, 669−679.
(55) Becker, E. D.; Liddel, U.; Shoolery, J. N. Nuclear Magnetic Resonance Studies of Hydrogen Bonding in Ethanol. *J. Mol. Spectrosc.* **1958**, *2*, 1−8.
(56) Dais, P.; Gibb, V.; Kenney-Wallace, G. A.; Reynolds, W. F. Molecular Relaxation Processes in Very Dilute Systems: A ^{13}C NMR Study of Alcohols in Alkanes. *Chem. Phys.* **1980**, *47*, 407−415.